Folding RNA into Function: The Art of Designing Functional RNA Origami

Luca Monari, Kerstin Göpfrich*

CSC Graduate School, Max Planck Institute for Medical Research

Supporting Information is available at https://lmonari5.github.io./

ABSTRACT: DNA origami has shown great potential in various applications such as synthetic biology, drug delivery, and materials science. However, the synthesis and functionalization of DNA origami structures are often incompatible with a cellular environment. RNA nanotechnology has emerged as a complementary tool that allows the formation of nanostructures within living or artificial cells. In this study, we aimed to design and construct two types of functional RNA origami: an RNA nanopore and an RNA filament. We used the RNA Origami Automated Design (ROAD) software to generate the DNA templates for co-transcriptional folding of RNA origami[1]. We then transcribed the RNA using a one-pot reaction and characterized the resulting structures using atomic force microscopy (AFM). Our results demonstrate the potential of RNA origami to synthesize functional full-RNA nanostructures in isothermal conditions. We thus lay the foundations to realize genetically encoded molecular hardware for synthetic cells.

INTRODUCTION

Is it possible to convert DNA origami to RNA origami? DNA nanotechnology is a rapidly developing field that has shown great potential in various applications such as synthetic biology, drug delivery, and materials science[2]. In particular, DNA origami can be precisely controlled and functionalized, thanks to the well-known potential energy landscape for DNA folding. However, the function of DNA origami structures often relies on chemical functionalization. DNA nanopores, for instance, have been modified with cholesterol-tags to enable their insertion into lipid membranes[3]. The chemistry of covalently linking a DNA strand to a cholesterol tag is not compatible with the cellular environment. RNA origami has been developed along parallel lines, however, it has so far never been employed in the context of synthetic biology. It may unlock the synthesis and functionalization of nanostructures within living or artificial cells. RNA nanotechnology has made significant progress in recent years, allowing for the design of a wide range of nanostructures and RNA aptamer motifs[4].

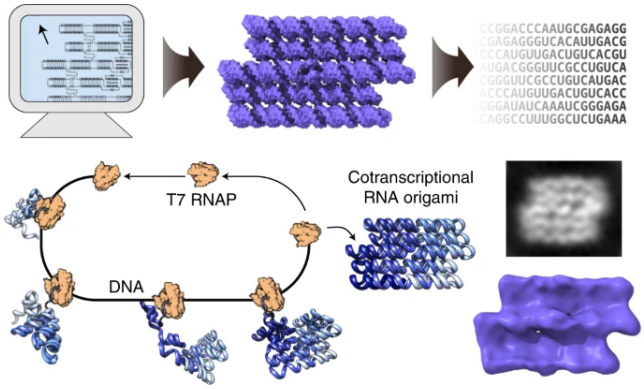

Figure 1. RNA Origami Automated Design software's pipeline and co-transcriptional folding scheme.

The RNA Origami Automated Design (ROAD) software allows for the design of RNA origami for co-transcriptional folding from a single DNA template[1], which can be synthesized without the need for thermal annealing and is therefore compatible with cellular environments. In addition, the wealth of aptamers available for RNA allows for the design of nanostructures with various functions, such as protein-RNA interactions[5], gene regulation[6], and enzymatic activity[7].

In this work, we aim to design and construct two types of functional RNA origami structures: an RNA nanopore and an RNA filament. Both of these functionalities have already been implemented with DNA nanotechnology[3,8], but the thermal annealing and the chemical functionalization required for DNA origami is not compatible with the synthesis in synthetic cells. Furthermore, RNA aptamers can replace DNA functionalization, leading to full-RNA nanostructures[5,9–11].

In this project, we use the ROAD software to generate the origami sequences and employ molecular dynamics (MD) relaxation to check the stability of the structures using oxDNA software[12–14,14,15]. We amplify the ordered DNA template using Polymerase Chain Reaction (PCR) and transcribe the RNA isothermally. We will then use agarose and PAGE gel electrophoresis, as well as atomic force microscopy (AFM) to characterize the transcribed

RNA and confirm correct folding. Finally, we use confocal microscopy to visualize the filaments assembly or the dye influx into lipid vesicles induced by the RNA nanopore.

RNA ORIGAMI DESIGN

The design of RNA origami is based on a single RNA strand that folds intramolecularly, like proteins do, into double helices and simple structural motifs. As such, RNA origami is fundamentally different from DNA origami, where multiple strand come together to form a desired shape. The RNA double helix differs from the common DNA structure due to the presence of an alcohol group in the 2' position of ribose, which forces the nucleotide into a bent conformation called the C3′-endo pucker. This results in a shorter phosphate-phosphate distance in the backbone and a more compact, A-shaped helix with a periodicity of 11 bases and a diameter of approximately 23 Å. Two helices can be designed using double-crossovers (DX) to arrange the RNA helices in parallel to form a building block (Figure 2A). When two DX are present in the same helix, the difference in base pairs between them is called a dovetail seam (DT). The dovetail is a key structural element as it determines the angle and vertical alignment between connected helices (Figure 2B-C, Table 1).

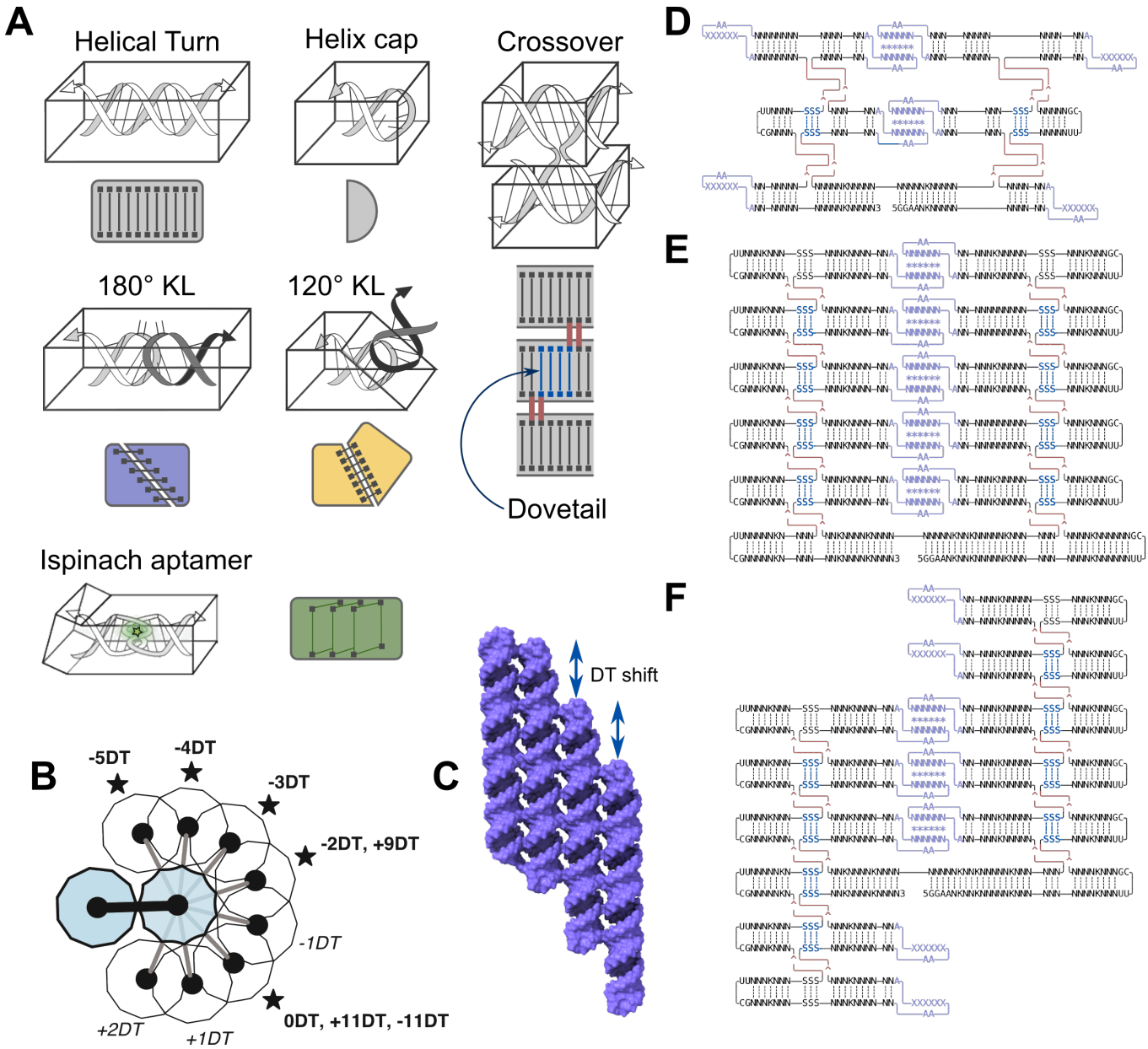

Figure 2. A) Building blocks for RNA origami design. B) Angles between helices induced by different dovetails. The DT number indicates the base pairs between two crossovers from the 5' to 3' direction. C) An example of helices shift induced by dovetail, using two dovetails of +10 bp. D) The ROAD RNA blueprint input for the filament tile. E) The ROAD RNA blueprint input for the six helices nanotube. F) The ROAD RNA blueprint input for the six helices nanotube with the zip design.

Table 1. Summary table of angles and helices doe to dovetails base pairs. The numbers are approximative values obtained from the ROAD RNAbuild software output.

DT	*Angle (°)*	*Shift (Å)*
-11	-145	24
-10	-110	21
-9	-80	19
-5	+50	7
-4	+90	5
-3	+120	2
-2	+150	-1
-1	-180	-4
0	-140	-7
+1	-110	-10
+2	-80	-12
+6	+50	-23
+7	+90	-26
+8	+120	-29
+9	+150	-32
+10	-180	-35
+11	-140	-38

A helix usually ends with a four-base hairpin loop to cap the structure, with the sequence UUCG being the most stable tetraloop. Hairpin loops with exposed bases, known as kissing stem-loop (KL), can also connect two helices with complementary sequences. ROAD supports 180° KL (composed of 6 bases) and 120° KL (composed of 7 bases). These structural elements, in combination with the library of compounds tested by Geary et al., allow for the design of a wide range of diverse RNA origami. Thus far, a variety of static non-functional 2D shapes have been made from DNA origami.

In this project, our aim is to go beyond the state-of-the art by designing 3D RNA origami and exploring the possibility to transition from structure to function, by making an RNA origami nanopore and an RNA filament.

The design of the RNA filament was based on the work of Rothemund et al., who developed programmable DNA nanotubes[8]. In the context of bottom-up synthetic biology, DNA nanotubes have been used as mimics of cytoskeletons inside of lipid vesicles[16], but they have never been synthesized inside of the vesicles. This limitation could be overcome by co-transcriptional folding of RNA origami, as described by Geary et al.. Both, Rothemund[8] and Geary[17] used tiles that assembled into larger structures, with DNA tiles relying on sticky ends and overhangs (interacting by base pairing) and co-transcriptional RNA origami self-assembly driven by kissing loop interactions. We designed RNA origami tiles with 3 helices and a dovetail of -3 bp to build a hexagonal nanotube (Figure 2D, Frames S1.1-3.1). The first and last helices were not capped, but external kissing loops were designed for the tile's self-assembly. To fluorescently track the RNA origami folding, we added the Ispinach aptamer into the design[18] (Frame S1.2-3.2). It has a G-quadruplex structure that greatly enhances the fluorescence signal of 3,5-difluoro-4-hydroxybenzylidene imidazolinone (DFHBI). We tested the formation of the nanotube first computationally using a short relaxation with OxDNA[19] (Frame S1.3).

The design of the RNA nanopore posed a significant challenge due to structural constraints. Our initial approach involved utilizing the angles imposed by dovetails to construct a small hexagonal nanotube (-3bp dovetails, 120°, Figure 2E, Frame S2.1-3.3). Such a design would feature an inner pore diameter of approximately 25 Å. While the structure predicted by ROAD was consistent with a nanopore, the formation of the nanotube solely depended on the angles of the dovetails. To ensure the successful folding of the nanotube, we implemented a "zip" structure in which the top and bottom parts of the RNA origami rolled in opposite directions, interacting with kissing loops (Figure 2F, Frame S2.2-3.4). However, upon analyzing the ROAD output for this design, we found that the top and bottom parts of the origami did not match perfectly due to the dovetail shift.

Therefore, we searched for a new design strategy based on two criteria: the angles of the dovetails should form a closed polygon, and we should minimize the helices shift induced by the dovetails. The formula for closed polygons is as follows:

$$(n-2) * 180 = \sum ai$$

where n is the number of sides/helices and ai is the internal angle of each dovetail. To minimize helices shift, the sum of the shifts induced by each dovetail (s_i) should be equal to 0:

$$\sum s_i = 0$$

We varied the number of helices (n) and the combination of dovetails (s_i and ai) to find the optimal design. The best we obtained was a structure with 8 helices and alternating dovetails of +9bp and -14bp (Frame S3.5). Many designs could be generated considering different kissing loops for the zipping (Frame S3.6).

Once we had designed the structure of the nanopore, we needed to ensure its insertion into the membrane. DNA and RNA origami often use numerous overhangs to bind cholesterol-functionalized DNA strands, but this approach is not suitable for co-transcriptional folding RNA origami. It is composed of a single strand and only has two overhangs (5' and 3') available for binding. Instead, we considered using RNA sequences known to bind GUV membranes, called RNA9, RNA10, and RNA13[10,11]. We attempted to incorporate our design with four RNA9 moieties, but it was not possible to synthesize DNA gene fragments with such long repeated sequences. Therefore, we designed eight kissing loops to interact and bind the RNA9, allowing it to drive the insertion of the

nanopore (Frame S3.7). Given a GUV membrane thickness of 5 nm and an approximate length of 12 nm for RNA9, we placed the attachment point for the RNA9 20 nanometers into the nanopore, ensuring full insertion. The ROAD's input and the 3D structures can be rendered and visualized in the supporting information.

MATERIALS AND METHODS

OxDNA relaxations. A Monte Carlo simulation of 1e4 steps (dt 0.05) with a canonical ensemble (NVT, 20°C) was run to avoid clashes or pseudoknots from the PDB file produced by ROAD. The interaction type was set 'RNA_relax', with harmonic force and high salt concentration. Then, a Molecular Dynamics NVT simulation ran for 1e7 steps (dt 0.0003) at 20°C. The interaction type was set 'RNA2' at high salt concentration, allowing wobble base pairs.

PCR amplification and purificiation. DNA templates were commercially synthesized (Integrated DNA Technologies) as double-stranded gBlocks. DNA gBlocks were PCR-amplified using 19–20-nt primers (Tm ≈ 53 °C) complementary to the ends of the gBlock, using standard Taq DNA polymerase from New England Biolabs, then purified using a Qiagen PCR purification kit.

RNA filament in vitro transcription. RNAs were transcribed and cotranscriptionally folded in a one-pot reaction containing template DNA (~5 ng µl−1 final), 6 mM Mg(OAc)2, 40 mM Na OAc, 40 mM KCl, 50 mM Tris-OAc (pH 7.8), rNTPs (0.5 mM each) and 1 mM dithiothreitol (DTT). Reactions were initiated by adding T7 RNA polymerase (~0.2 U/50 µl). Transcription reactions were carried out in 50-µl volumes at 37.0 °C for 45 min to 2 h, depending on the sequence length. Larger designs required longer synthesis times (1–2 h), whereas smaller designs (for example 2AE) required just a few minutes to reveal multimeric products by AFM.

RNA nanopore in vitro transcription optimization. The RNA nanopore transcription was optimized because it was not possible to amplify the gene fragments with high accuracy (Table 2, Fig. 3). Different conditions were designed considering both the work of Kartje et al.[20] and the buffer for the RNA9 membrane binding (50 mM HEPES at pH 7.0, 50 mM NaCl, 5 mM MgCl2, 2 mM CaCl2). Each transcription was performed in 50 uL with 1 uL of T7 RNA polymerase (~ 20 U) from Sigma-Aldrich. The stock T7 RNA polymerase stock solution also contains 10 mM potassium phosphate, 200 mM KCl, 0.1 mM EDTA, 30 mM 2-mercaptoethanol, 50% glycerol (v/v), 0.1% Tween 20, pH 7.9. We tried to change the conditions from the kit transcription buffer to the binding buffer, using Hepes-NaOH and Tris-HCl buffers at pH 7.3. The presence of NaCl, below 70 mM, increases the transcription efficiency and helps the RNA origami folding. On the contrary, calcium ions highly inhibit transcription.

In the end, the most efficient transcription condition was the kit buffer with 50 mM of NaCl.

Table 2. Transcription optimization conditions. The sodium concentration marked with * indicated that the salt concentration from the buffer solution was taken into account. Sample I** doesn't contain T7-polymerase.

	Tris-HCl pH 7.9 (mM)	*Tris-HCl pH 7.3 (mM)*	*MgCl2 (mM)*	*DTT (mM)*	*Spermidine (mM)*	*NaCl (mM)*	*CaCl2 (mM)*	*Hepes pH 7.3 (mM)*	*DNA (ng/uL)*
A	40	/	6	10	2	/	/	/	/
B	40	/	6	10	2	/	/	/	5
C	/	40	6	10	2	50	/	/	5
D	/	40	6	10	2	50	/	/	5
E	/	40	6	/	/	50*	/	/	5
F	/	/	6	/	/	50	/	50	5
G	/	/	6	/	/	50*	/	50	5
H	/	/	1	/	/	50*	2	50	5
*I***	40	/	6	10	2	/	/	/	5
J	40	/	6	10	2	/	/	/	5
K	40	/	6	10	2	/	/	/	/
L	40	/	6	10	2	50	/	/	5
M	40	/	6	10	2	50	2	/	5
N	/	40	6	/	/	50*	2	/	5
O	/	/	6	/	/	50	2	50	5
P	/	/	6	/	/	50*	2	50	5
Q	/	/	1	/	/	50*	7	50	5

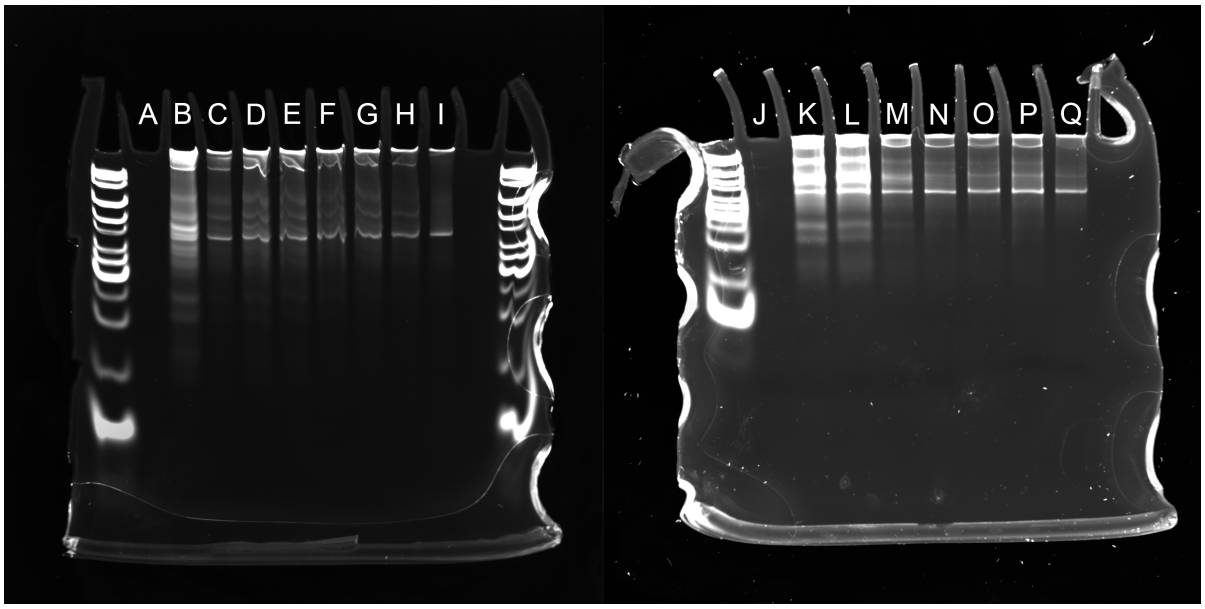

Figure 3. Transcription optimization PAGE gels

AFM imaging. All samples were mixed with the imaging buffer (1X TAE, 20mM MgCl2) at 1:1 ratio. The mix was then deposited on a cleaved mica and incubated for 1 min at room temperature. The chamber was then filled with 1mL of the imaging buffer. The chamber was then imaged at room temperature using a NanoWizzard 2 high speed AFM (Bruker) in fast imaging AC mode with a Fast Scan D cantilever (Bruker).

Agarose gel electrophoresis. 1.5 grams of agarose were dissolved in 100 mL of 1.5x TBE and 6mM MgCl2. The mixture was heated until boiling, let cool down to 60°C and poured into the gel tray with the comb. To prepare the samples, 10 uL of RNA origami solution were mixed with 2 uL of 6x Tillibit Loading Dye. After the gel was cooled down, 10 uL of each sample was loaded. As a reference, we loaded Quick-Load® 1 kb DNA Ladder, purchased from New England BioLabs. The gel ran for 3.5-5h at 60 V, ~130mA. In the end, the gel was stained with GelRed on the rocking table for 20 min and imaged with UV light at different exposures using an Azure C600.

Polyacrylamide gel electrophoresis (PAGE). 15 ml of polyacrylamide gel was prepared by mixing 7.66 ml Water, 1.5 ml TBE 10x, 135 uL MgCl2 1M, 5.63 ml acrylamide 40%, 75 uL ammonium persulfate (APS) 10% m/m, 5 uL tetramethylethylenediamine (TEMED). The solution was fastly poured into the gel tray with the comb. To prepare the samples, 10 uL of RNA solution were mixed with 2 uL of 6x Tillibit Loading Dye. After the gel was cooled down, 10 uL of each sample was loaded. As a reference, we loaded TriDye™ Ultra Low Range DNA Ladder, purchased from New England BioLabs. The gel ran for 2.5-4h at 100 V, ~18-22 mA. In the end, the gel was stained with GelRed on the rocking table for 20 min and imaged with UV light at different exposures using an Azure C600.

GUV formation. 1,2-dioleoyl-sn-glycero-3-phosphocholine (18:1 DOPC) was purchased from Avanti Polar Lipids, Inc. and 1,2-Dioleoyl-sn-glycero-3-phosphoethanolamine fluorescently labeled with ATTO 390(DOPE-ATTO390) was purchased from ATTO-TEC. Both were stored in CHCl3 at −20 °C. Giant Unilamellar Vesicles (GUVs) were produced via the electroformation method using a VesiclePrepPro device (Nanion Technologies GmbH). 40 µL of 1 mM lipid mix (containing 99 % DOPC and 1 % DOPE-ATTO390) in CHCl3 were homogeneously spread on the conductive side of an indium tin oxide (ITO) coated glass slide (Visiontek Systems Ltd) using a cover slide. The lipid-coated ITO slide was subsequently placed under vacuum for at least 30 min to achieve complete evaporation of the CHCl3. A rubber ring with a diameter of 18 mm was placed on the lipid-coated ITO slide. The ring was filled with 275 µL of 390 mM sucrose solution, before creating a sealed chamber by placing a second ITO slide on top. The assembled electroformation chamber was placed into the VesiclePrepPro and connected to the electrodes. An AC field (3 V, 5 Hz) was applied across the ITO slides for 126 min while heating the solution to 37 °C. GUVs were collected immediately after formation and stored at 4 °C for up to 7 days.

Confocal microscope imaging. The glass slides for imaging are passivated with Bovine Serum Albumin (BSA) 20 mg/L for 15 min. The solution is deposited in the observation chamber and then sealed to reduce airflow. A confocal laser scanning microscope LSM 900 (Carl Zeiss AG) was used for confocal microscopy. The pinhole aperture was set to one Airy Unit, and the experiments were performed at room temperature. The images were acquired using a 20× (Plan-Apochromat 20×/0.8 air M27, Carl Zeiss AG) objective. Images were

analyzed and processed with ImageJ (NIH, brightness and contrast adjusted).

RESULTS

We used atomic force microscopy (AFM) to visualize the transcribed RNA origami on a mica surface in the presence of Mg2+ ions. Mg2+ ions immobilize and adsorb the negatively charged DNA and RNA nanostructures on the surface. In particular, three-dimensional DNA origami structures open and flatten due to the strong interaction with the mica. Also, it is worth noticing that the AFM cantilever scans the sample by tapping the surface, which may result in the helices' heights being lower than expected and the dimensions of the origami slightly altered due to artifacts. Therefore, the AFM images provide an approximate representation of the 2D structure of the origami.

In Figure 4A-C, we show the RNA filament tiles in the presence and absence of the Ispinach aptamer. The transcribed tiles with Ispinach (Fig. 4A) led to the formation of filaments reaching a length up to 500 nm and a width of approximately 20 nm, corresponding roughly to two tiles. It matches our design of four helices per tile (helix width is around 2.4 nm). In contrast, the tiles without aptamers produced much shorter and more flexible filaments. Figure 4B shows the filaments before purification at high concentrations, where numerous bundles are present. After spin filtration, the filament

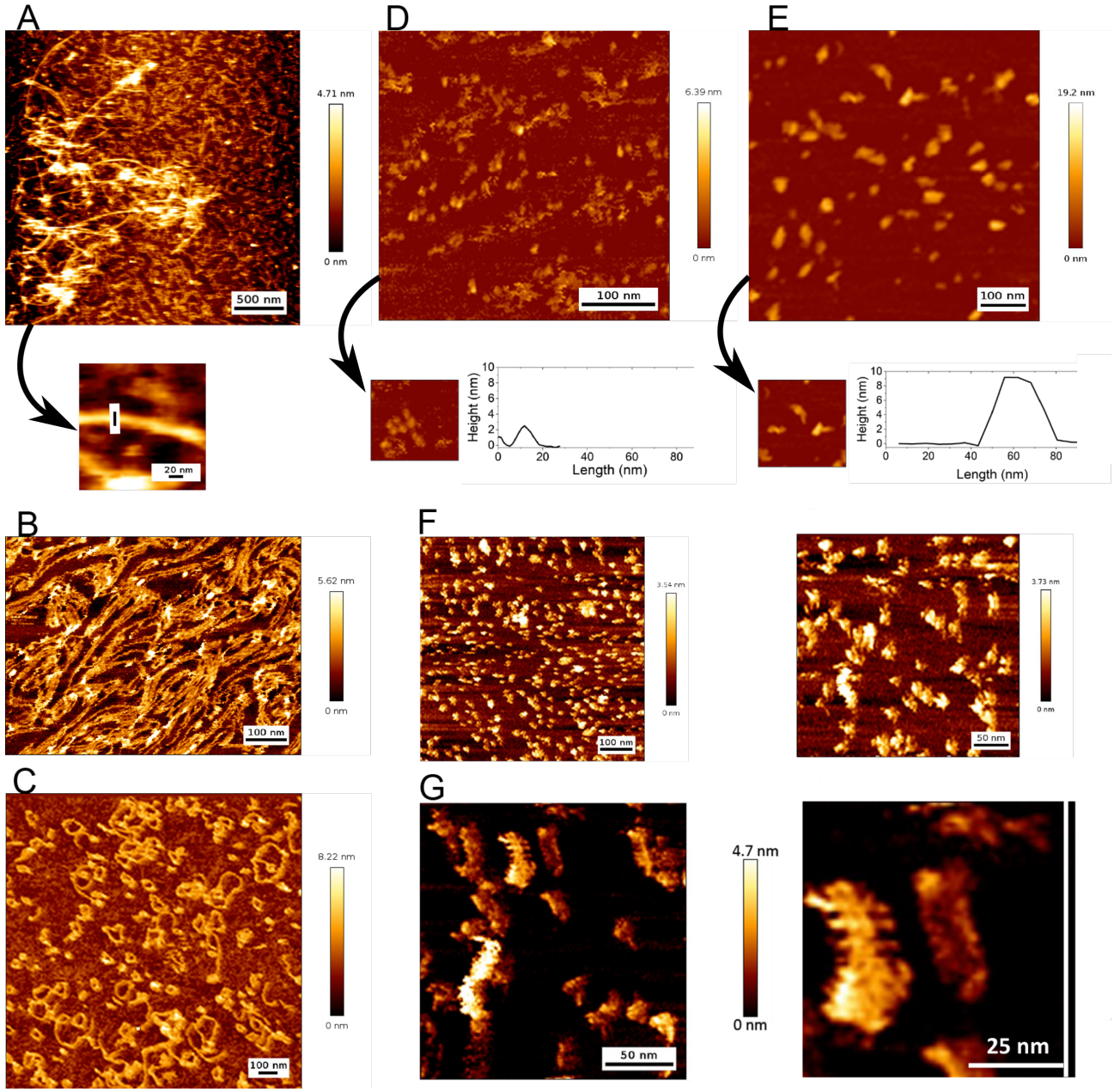

Figure 4. AFM imaging of RNA origami. A) RNA tiles with Ispinach. B) RNA tiles without Ispinach aptamer. C) RNA tiles after purification. D) RNA nanotube with six helices. E) RNA nanotube with six helices and zip design. F) RNA nanotube with eight helices, zip design and kissing loops for RNA9. G) RNA 8 helices nanotube damaged/with artifacts.

remained highly flexible and often formed closed rings (Fig. 4C). These results suggest that the Ispinach aptamer may contribute to filament stiffness, preventing tiles from wrong assembly, likely due to steric hindrance effects.

In our nanopore project, we first used atomic force microscopy (AFM) to image the hexagonal nanopore designs (Fig. 4D-E). These structures are quite small, with the open nanotube measuring approximately 15x17 nm, making them more difficult to image with AFM. However, we were still able to observe numerous structures with dimensions similar to what we expected. The average height measured was approximately 2 nm, which corresponds to an RNA helix slightly compressed by the AFM cantilever (Fig. 4D). We also imaged the zip equivalent of the hexagonal design and found structures with similar lengths. Interestingly, we measured an average height ranging from 7 to 9 nm, which suggests the formation of nanotubes (Fig. 4E).

Next, we attempted to amplify gene fragments for the 8H nanopore using polymerase chain reaction (PCR). However, we were unsuccessful due to impurities in the stock solutions. Therefore, we performed transcription at a lower template concentration (10 ng) for a longer time (5 h). After AFM imaging, we observed structures with dimensions close to what we expected (40x20 nm, Fig. 4F). Although some of the RNA origami appeared to be damaged, it is difficult to image with precision on the nanometer scale without introducing artifacts (Fig. 4G).

After verifying the production of the RNA origami, we were ready to conduct influx experiments in giant unilamellar vesicles (GUV). Before running the main influx experiment, we performed negative controls using the transcription buffer and fluorescein sodium salt as an external dye (MW 376.27 g/mol). Fluorescein is known to not be permeable to membranes. In the negative control experiments, we observed permeability of the GUVs (Fig. 5). We repeated the experiment with Alexa647 (MW 4,880.7 g/mol) and again observed an influx. Therefore, before proceeding with the influx experiment, we are planning to purify the RNA origami to prevent GUV permeability induced by components present in the transcription buffer.

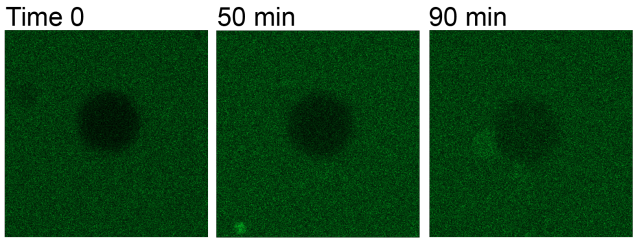

Figure 5. Example of a GUV showing influx with the control buffer.

CONCLUSIONS

The design of functional RNA origami has garnered significant attention as a promising approach in molecular biology and nanotechnology. New software, such as ROAD, enables the generation of complex, functional structures at the nanoscale. In this study, we used ROAD and molecular dynamics relaxation to generate and test the stability of our RNA origami designs. While current tools have enabled the successful production of co-transcriptional RNA origami with desired three-dimensional structures, the design of functional RNA origami remains a challenge that requires further exploration.

We were able to encode filament assembly in our origami design, but further optimization is necessary to achieve longer lengths. Our goal was to use the RNA origami building blocks to force the formation of a nanotube and ultimately build a full-RNA nanopore. Further experiments, such as RNA purification and influx, are needed to demonstrate the functionality of the structure.

In summary, this research highlights the potential of using RNA origami as a powerful tool for synthesizing functional nanostructures within living cells or artificial vesicles. The ability to design nanostructures with diverse functions using RNA aptamers, combined with the RNA Origami Automated Design software's capability for co-transcriptional folding, makes RNA origami a promising development for synthetic biology and materials science. The combination of RNA's versatility with the nanoscale precision of DNA origami could pave the way for new advances in the creation of synthetic cells and other applications.

AUTHOR CONTRIBUTION

M. Tran and K. Goepfrich conceived the idea behind the filament project. L. Monari designed the RNA origami tiles following the requirements of M. Tran and performed OxDNA simulation with the help of E. Poppleton. The experiments for the filament project were carried out by M. Tran. The nanopore project was conceived by Kerstin Goepfrich and designed with the help of L. Monari and A. Griffo. L. Monari designed the nanopore structures. The OxDNA relaxations were performed by L. Monari with the suggestions of E. Poppleton. The experimental procedure (RNA transcription, GUV electroformation, PCR amplification, PAGE and agarose gel, confocal microscope imaging) were carried out by L. Monari and A. Griffo. The AFM imaging was performed by M. Tran and A. Griffo.

ACKNOWLEDGMENT

I want to express my deepest gratitude to Kerstin Göpfrich for her support and guidance. What she taught me goes far beyond science. I'm also extremely grateful to A. Griffo and M. Tran for their patience, helping me move the first steps towards biophysics. Many thanks should also go to E. Poppleton, his help has been essential. Thanks to M. Illing, for all the tips on GUVs and for answering all my questions. I am also grateful to all the other group members for welcoming me inside and outside the lab.

REFERENCES

(1) Geary, C.; Grossi, G.; McRae, E. K. S.; Rothemund, P. W. K.; Andersen, E. S. RNA

Origami Design Tools Enable Cotranscriptional Folding of Kilobase-Sized Nanoscaffolds. *Nat. Chem.* **2021**, *13* (6), 549–558. https://doi.org/10.1038/s41557-021-00679-1.

(2) Dey, S.; Fan, C.; Gothelf, K. V.; Li, J.; Lin, C.; Liu, L.; Liu, N.; Nijenhuis, M. A. D.; Saccà, B.; Simmel, F. C.; Yan, H.; Zhan, P. DNA Origami. *Nat. Rev. Methods Primer* **2021**, *1* (1), 13. https://doi.org/10.1038/s43586-020-00009-8.

(3) Jahnke, K.; Illig, M.; Scheffold, M.; Tran, M. P.; Mersdorf, U.; Göpfrich, K. *Mechanochemical Signal Transduction in Synthetic Cells*; preprint; Biophysics, 2022. https://doi.org/10.1101/2022.04.26.489423.

(4) Adachi; Nakamura. Aptamers: A Review of Their Chemical Properties and Modifications for Therapeutic Application. *Molecules* **2019**, *24* (23), 4229. https://doi.org/10.3390/molecules24234229.

(5) Liu, S.; Li, B.; Liang, Q.; Liu, A.; Qu, L.; Yang, J. Classification and Function of RNA –Protein Interactions. *WIREs RNA* **2020**, *11* (6). https://doi.org/10.1002/wrna.1601.

(6) Schaffter, S. W.; Schulman, R. Building in Vitro Transcriptional Regulatory Networks by Successively Integrating Multiple Functional Circuit Modules. *Nat. Chem.* **2019**, *11* (9), 829–838. https://doi.org/10.1038/s41557-019-0292-z.

(7) Westhof, E.; Lescoute, A. Ribozymes. In *Encyclopedia of Virology*; Elsevier, 2008; pp 475–481. https://doi.org/10.1016/B978-012374410-4.00495-7.

(8) Rothemund, P. W. K.; Ekani-Nkodo, A.; Papadakis, N.; Kumar, A.; Fygenson, D. K.; Winfree, E. Design and Characterization of Programmable DNA Nanotubes. *J. Am. Chem. Soc.* **2004**, *126* (50), 16344–16352. https://doi.org/10.1021/ja044319l.

(9) Janas, T. Specific RNA Binding to Ordered Phospholipid Bilayers. *Nucleic Acids Res.* **2006**, *34* (7), 2128–2136. https://doi.org/10.1093/nar/gkl220.

(10) Janas, T.; Yarus, M. Visualization of Membrane RNAs. *RNA* **2003**, *9* (11), 1353–1361. https://doi.org/10.1261/rna.5129803.

(11) Khvorova, A.; Kwak, Y.-G.; Tamkun, M.; Majerfeld, I.; Yarus, M. RNAs That Bind and Change the Permeability of Phospholipid Membranes. *Proc. Natl. Acad. Sci.* **1999**, *96* (19), 10649–10654. https://doi.org/10.1073/pnas.96.19.10649.

(12) Bohlin, J.; Matthies, M.; Poppleton, E.; Procyk, J.; Mallya, A.; Yan, H.; Šulc, P. Design and Simulation of DNA, RNA and Hybrid Protein–Nucleic Acid Nanostructures with OxView. *Nat. Protoc.* **2022**, *17* (8), 1762–1788. https://doi.org/10.1038/s41596-022-00688-5.

(13) Poppleton, E.; Bohlin, J.; Matthies, M.; Sharma, S.; Zhang, F.; Šulc, P. Design, Optimization and Analysis of Large DNA and RNA Nanostructures through Interactive Visualization, Editing and Molecular Simulation. *Nucleic Acids Res.* **2020**, *48* (12), e72–e72. https://doi.org/10.1093/nar/gkaa417.

(14) Šulc, P.; Romano, F.; Ouldridge, T. E.; Rovigatti, L.; Doye, J. P. K.; Louis, A. A. Sequence-Dependent Thermodynamics of a Coarse-Grained DNA Model. *J. Chem. Phys.* **2012**, *137* (13), 135101. https://doi.org/10.1063/1.4754132.

(15) Rovigatti, L.; Šulc, P.; Reguly, I. Z.; Romano, F. A Comparison between Parallelization Approaches in Molecular Dynamics Simulations on GPUs. *J. Comput. Chem.* **2015**, *36* (1), 1–8. https://doi.org/10.1002/jcc.23763.

(16) Jahnke, K.; Huth, V.; Mersdorf, U.; Liu, N.; Göpfrich, K. Bottom-Up Assembly of Synthetic Cells with a DNA Cytoskeleton. *ACS Nano* **2022**, *16* (5), 7233–7241. https://doi.org/10.1021/acsnano.1c10703.

(17) Geary, C.; Rothemund, P. W. K.; Andersen, E. S. A Single-Stranded Architecture for Cotranscriptional Folding of RNA Nanostructures. *Science* **2014**, *345* (6198), 799–804. https://doi.org/10.1126/science.1253920.

(18) Autour, A.; Westhof, E.; Ryckelynck, M. ISpinach: A Fluorogenic RNA Aptamer Optimized for *in Vitro* Applications. *Nucleic Acids Res.* **2016**, *44* (6), 2491–2500. https://doi.org/10.1093/nar/gkw083.

(19) Šulc, P.; Romano, F.; Ouldridge, T. E.; Doye, J. P. K.; Louis, A. A. A Nucleotide-Level Coarse-Grained Model of RNA. *J. Chem. Phys.* **2014**, *140* (23), 235102. https://doi.org/10.1063/1.4881424.

(20) Kartje, Z. J.; Janis, H. I.; Mukhopadhyay, S.; Gagnon, K. T. Revisiting T7 RNA Polymerase Transcription in Vitro with the Broccoli RNA Aptamer as a Simplified Real-Time Fluorescent Reporter. *J. Biol. Chem.* **2021**, *296*, 100175. https://doi.org/10.1074/jbc.RA120.014553.